MDPI

Article

Development of Flow Fields for Zinc Slurry Air Flow Batteries

Nak Heon Choi [1,2,*], Diego del Olmo [3], Peter Fischer [1], Karsten Pinkwart [1,4] and Jens Tübke [1,2]

[1] Applied Electrochemistry, Fraunhofer Institute for Chemical Technology ICT, Joseph-von-Fraunhofer, Straße 7, 76327 Pfinztal, Germany; peter.fischer@ict.fraunhofer.de (P.F.); karsten.pinkwart@ict.fraunhofer.de (K.P.); jens.tuebke@ict.fraunhofer.de (J.T.)

[2] Institute for Mechanical Process Engineering and Mechanics, Karlsruhe Institute of Technology KIT, Straße am Forum 8, 76131 Karlsruhe, Germany

[3] Department of Chemical Engineering, University of Chemistry and Technology Prague, Technická 5, 16628 Prague 6, Czech Republic; Diego1.Del.Olmo.Diaz@vscht.cz

[4] Faculty of Electrical Engineering and Information Technology, Karlsruhe University of Applied Sciences, Moltkestraße 30, 76133 Karlsruhe, Germany

* Correspondence: nak.choi@ict.fraunhofer.de; Tel.: +49-721-4640-827

check for updates

Abstract: The flow field design and material composition of the electrode plays an important role in the performance of redox flow batteries, especially when using highly viscous liquids. To enhance the discharge power density of zinc slurry air flow batteries, an optimum slurry distribution in the cell is key. Hence, several types of flow fields (serpentine, parallel, plastic flow frames) were tested in this study to improve the discharge power density of the battery. The serpentine flow field delivered a power density of 55 mW·cm^{-2}, while parallel and flow frame resulted in 30 mW·cm^{-2} and 10 mW·cm^{-2}, respectively. Moreover, when the anode bipolar plate material was changed from graphite to copper, the power density of the flow frame increased to 65 mW·cm^{-2}, and further improvement was attained when the bipolar plate material was further changed to copper–nickel. These results show the potential to increase the power density of slurry-based flow batteries by flow field optimization and design of bipolar plate materials.
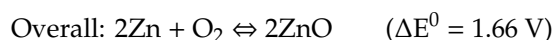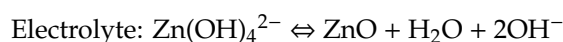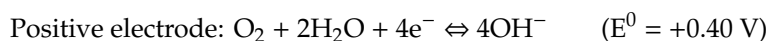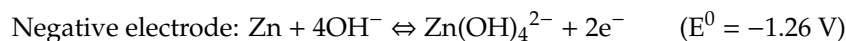
1. Introduction

Recently, there was an extensive amount of research on energy storage systems in combination with renewable energies such as solar energy, wind energy, and wave energy. One of the most promising candidates includes redox flow batteries (RFBs), which are gaining attention due to their flexibility in the layout of capacity and power [1–3]. The energy densities of RFBs are determined by the volume of electrolyte used and concentration of active species, whilst the power densities can be improved by electrode size and performance [4,5]. Various RFB systems were investigated, including all-vanadium, hydrogen–bromine, and aqueous organic redox couples [5]. The zinc slurry air flow battery is one of the most promising battery chemistries among these, given its relatively higher theoretical energy density of 1350 Wh/kg [1]. Its high negative reduction potential and low cost, on account of its abundance, make zinc an attractive material for battery applications. Furthermore, zinc electrodes present advantages in terms of safety when compared, for example, to lithium- or bromine-based technologies [6–8]. Therefore, several types of zinc-based battery systems were developed [9], and primary zinc–air batteries are prevalent for certain applications [10]. However, rechargeable zinc battery technology faces several problems which are currently being investigated [11–13]. Problems

associated with material reorganization and the formation of dendrites could be prevented when using slurry-based configurations [14].

The zinc–air battery is based on zinc as an active static anode material and air flowing in the cathode [10]. During discharge, air flows in the positive electrode where the oxygen reduction reaction (ORR) takes place, while, in the negative electrode, the zinc oxidizes to zincate which can further decompose to zinc oxide in highly alkaline media [15]. Below are the main chemical reactions taking place on the zinc–air battery.

$$\text{Negative electrode: } Zn + 4OH^- \Leftrightarrow Zn(OH)_4^{2-} + 2e^- \qquad (E^0 = -1.26 \text{ V})$$

$$\text{Positive electrode: } O_2 + 2H_2O + 4e^- \Leftrightarrow 4OH^- \qquad (E^0 = +0.40 \text{ V})$$

$$\text{Electrolyte: } Zn(OH)_4^{2-} \Leftrightarrow ZnO + H_2O + 2OH^-$$

$$\text{Overall: } 2Zn + O_2 \Leftrightarrow 2ZnO \qquad (\Delta E^0 = 1.66 \text{ V})$$

Unlike conventional configurations, in zinc slurry air flow batteries, the anode is formed by zinc particles suspended in a highly alkaline electrolyte forming a slurry which can flow in and out of the system [8,16]. One of the main advantages of zinc slurry air flow batteries is their higher capacity compared to conventional zinc–air batteries. As the capacity of the battery is determined by the amount of active material in the slurry, it can be boosted by increasing the volume of the tank or amount of zinc in the slurry [17]. On the other hand, the current and power densities are determined by the flow of zinc slurry in the system. For zinc slurry air flow batteries, the electrolyte flow is an important factor because of the lack of a static electrode to provide additional surface area for the electrochemical reaction. In other words, carbon felts or other porous electrodes, which are used to increase surface area in other RFBs, are not present at the negative electrode of the zinc slurry air flow battery. This is because the slurry, consisting of zinc particles suspended in a highly alkaline electrolyte, acts as both electrode and electrolyte.

Several different aspects of the zinc slurry air flow battery are under active development, aiming to improve its electrochemical performance, such as catalyst research to enhance ORR kinetics [18,19] and zinc slurry formulation to improve the negative electrode performance [20,21]. Membranes or separators [22,23] are also important components of this system; as water is required in the ORR, the water transport from the zinc slurry plays a crucial role. Furthermore, the optimization of the flow field for the zinc electrode is key to improving the battery performance. This is because the flow field promotes uniform distribution of the zinc slurry over the geometric area surface of the bipolar plate, and it can help minimize mass transport polarization. Thus, the electrochemical performance of the cell can be enhanced by optimizing the flow field.

Extensive literature is available on the design and development of flow fields for RFBs based on dissolved species, such as vanadium redox flow batteries (VRFBs) [24–34]. For example, Xu et al. [31,32] performed numerical experiments in which the serpentine flow field showed higher power density compared to other types of flow field and a flow-through design. Furthermore, the study showed that the electrolytes were not evenly distributed throughout the electrode when parallel and flow-through configurations were used, which led to reduced round-trip efficiency. Dennison et al. [33] tested experimentally various types of flow fields (serpentine, parallel, interdigitated, and spiral) with two different types of porous electrode. Their results indicated that the serpentine flow field had the best electrochemical performance with both porous electrodes. Furthermore, they concluded that, unlike the other flow fields, the interdigitated flow field does not benefit from the use of perforated electrodes. For hydrogen–bromine RFBs, Cho et al. [34] studied numerically two different types of flow field with flow-by and flow-through configurations. Their results showed approximately 24% higher power density when flow-through configurations were used for hydrogen–bromine RFB. However, much less research was conducted on the optimization of flow fields for electrolytes based on solid–liquid mixtures such as slurries.

Herein, we introduce and test different types of anode flow fields in an in-house built cell to study how the flow distribution affects the electrochemical performance of the zinc slurry air flow battery. The cell performance is analyzed by determining the polarization behavior of the system and assessing the effect of charge transfer and ohmic resistances. Furthermore, we study the effect of bipolar plate conductivity by using different materials (graphite and metallic).

2. Materials and Methods

2.1. Air Cathode

The air cathode was prepared by the catalyst-coated electrode (CCE) method. The catalyst ink was prepared by mixing a Pt/C catalyst (40% Pt, Alfa Aesar, Kandel, Germany) with 10 wt% Fumion FAA-3 Ionomer (Fumatech, Bietigheim-Bissingen, Germany), deionized water, and isopropanol. This mixture was sonicated in an ultrasonic water bath for 15 min and then sprayed directly onto a gas diffusion layer (SGL Carbon, 29BC, Meitingen, Germany) with a geometric area of 25 cm^2 (5 cm × 5 cm × 0.0235 cm). The platinum loading was fixed at 1 mg·cm^{-2} and the ionomer content of the catalyst layer was set to 23 wt%.

2.2. Zinc Slurry Preparation

The zinc slurry was prepared by adding Carbopol TM 940 (Acros Organics, Nidderau, Germany) to 10 M KOH (Carl Roth, Karlsruhe, Germany). The solution was mixed by using a high shear homogenizer Yellow line, Ultra Turrax DI 25 basic (Ika, Staufen, Germany) at 11,000 rpm for 5 min to ensure a strong gel network by dispersing the gelling agent. Then, ZnO (VWR Chemicals, Dietikon, Switzerland) was added and mixed again by using the high shear homogenizer for 5 min. Finally, zinc powder with an average particle size of 50 μm (GC 7-4/200 Bi/200ln, Grillo, Duisburg, Germany) was added to the solution and mixed with the homogenizer for another 5 min. The total volume of zinc slurry was 70 mL, and the contents of the zinc slurry are shown in Table 1.

Table 1. Composition of the zinc slurry.

Mass Fraction (wt%)			
Zinc	ZnO	Carbopol	KOH + Water
33.8	4	0.7	61.5

2.3. Flow Field Design

In order to study the effect of the anode flow field on the single cell performance, different types of flow fields were designed as shown in Figure 1. For the cathode bipolar plate, a serpentine flow field (a) was chosen, whereas, for the anode graphite bipolar plate, as the reactant is viscous zinc slurry, wider serpentine (b), parallel, (c) flow fields, and a flow frame (d) were designed to assess the electrochemical performance of the system. The flow frame consists of a Polytetrafluoroethylene (PTFE) frame placed on the top of a flat bipolar plate, instead of manufacturing flow fields on the plate. Furthermore, to study the influence of the bipolar plate conductivity, a copper foil was placed on the top of graphite plate for the flow frame configuration (e). Lastly, a modified serpentine flow field was designed and manufactured using a copper–nickel (70:30) plate (CuNi30, NIEMET, Bremen, Germany) (f).
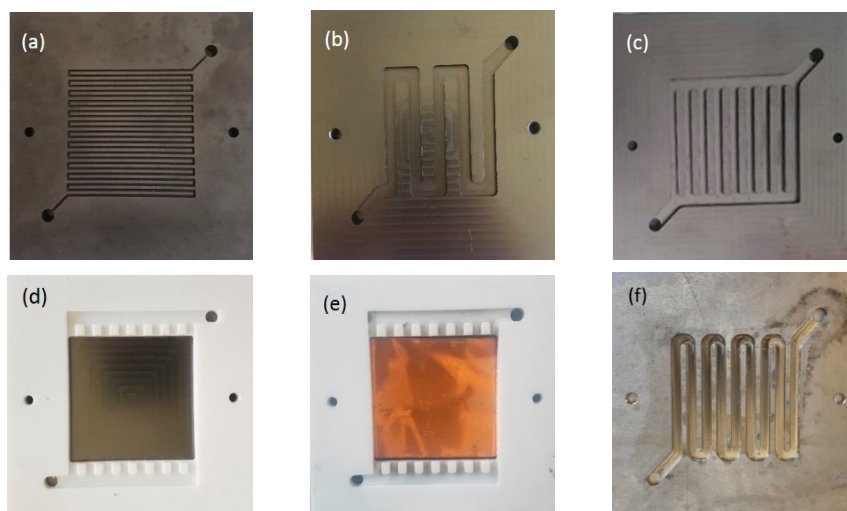
Figure 1. Flow fields used in this study. For the positive electrode: (**a**) serpentine. For the negative electrode: (**b**) serpentine, (**c**) parallel, (**d**) flow frame, (**e**) copper-based flow frame, and (**f**) modified serpentine.

2.4. Single Cell Assembly and Electrochemical Performance

A single cell was designed to study the electrochemical performance of zinc slurry air flow batteries. As shown in Figure 2, the single cell consists of an end plate, a current collector, bipolar plates with a geometric active area of 25 cm^2, gaskets, and a separator. A catalyst-coated electrode was placed between the separator (Cellophane™ PØØ purchased from FUTAMURA, Hamburg, Germany) and the cathode bipolar plate. When flow fields were used, no flow frame was present in the cell. After the single cell was assembled, it was used to determine the electrochemical performance of each flow field by means of current–voltage characteristic curves (polarization curves) by using a BaSyTec GSM Battery Test System (BaSyTec GmbH, Asselfingen, Germany) and electrochemical impedance spectroscopy (EIS) by using a Zahner IM6 workstation. The EIS measurements were carried out at 1.3 V and 1.0 V to assess the resistance of flow fields at different polarization. During the measurements, zinc slurry and synthetic air were constantly flowed in the anode and cathode compartments with a flow rate of 160 mL·min^{-1} and 100 mL·min^{-1}, respectively. The use of a slurry electrode resulted in voltage fluctuations while recording polarization curves. Hence, at each current density, the voltage was recorded for one minute and averaged.
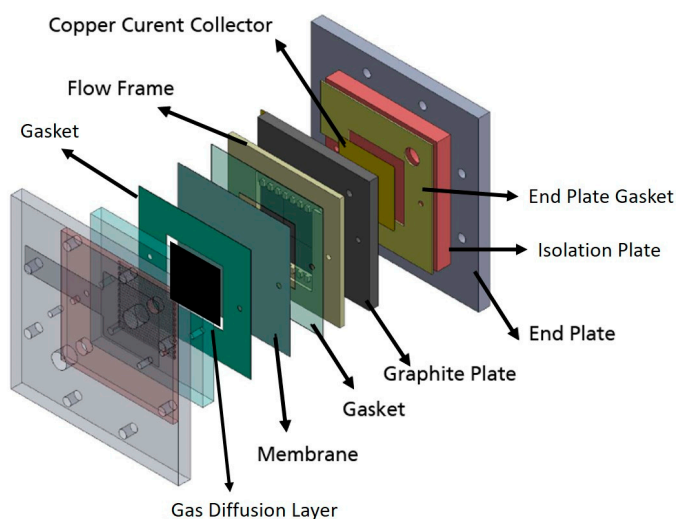

Figure 2. Schematic diagram of a single cell zinc slurry air flow battery with a flow frame.

3. Results and Discussion

3.1. Effect of Flow Fields

The polarization curves in Figure 3 show that, with graphite-based bipolar plates, the serpentine flow field exhibited higher current densities than the parallel type or the flow frame at 0.7 V with 75, 40, and 15 mA·cm^{-2}, respectively. Hence, the maximum power densities were 55, 30, and 10 mW·cm^{-2}, respectively. As the Nyquist plots in Figure 4 indicate, the ohmic resistive component of the impedance (where the curve intersects the real axis at high frequency) was almost the same for all flow fields except for the parallel type as shown in Figure 4c. The parallel flow field showed 0.2 Ω at 1.3 V and 0.12 Ω at 1.0 V, whereas the serpentine flow field and the flow frame showed around 0.09 and 0.1 Ω at 1.3 V, and 0.07 and 0.10 Ω at 1.0 V. However, there were more significant differences in the charge transfer resistance, as shown in Figure 4d. Unlike other RFB Nyquist plots, the plots presented in Figure 4 show oscillation due to the absence of a static electrode. This results in a constant variation of the electrochemically active area, due to the formation and breaking of percolation networks between the zinc particles in the slurry. Hence, the result was first fitted to the equivalent circuit shown in Figure 4a to calculate the charge transfer resistance. The flow frame had 10 times more charge transfer resistance at 1.3 V, 2.7 Ω, than the serpentine or parallel flow fields, around 0.25 Ω. At 1.0 V, the flow frame showed a resistance of 1.75 Ω, whereas the serpentine flow field showed 0.22 Ω and the parallel one showed 0.45 Ω.

All the flow fields under study had the same apparent geometric active area of 25 cm^2 but the actual geometric active area was different. For example, for the flow frame, the geometric and corrected active areas were equal as it was a flat planar surface. In other words, the zinc slurry flowed on the surface of the flat bipolar plate. However, both serpentine and parallel flow fields had paths for the slurry. In our design, as there was a gap between the flow field and the separator due to the gasket, the slurry could flow both through the path and over the walls; thus, the geometric area was still 25 cm^2. However, the zinc particles could also be discharged when they were in contact with the walls. Subsequently, even if the geometric area was the same for all flow fields, it had to be corrected to include the wall area, leading to differences between the designs. Details of the corrected geometric area are shown in Table 2.
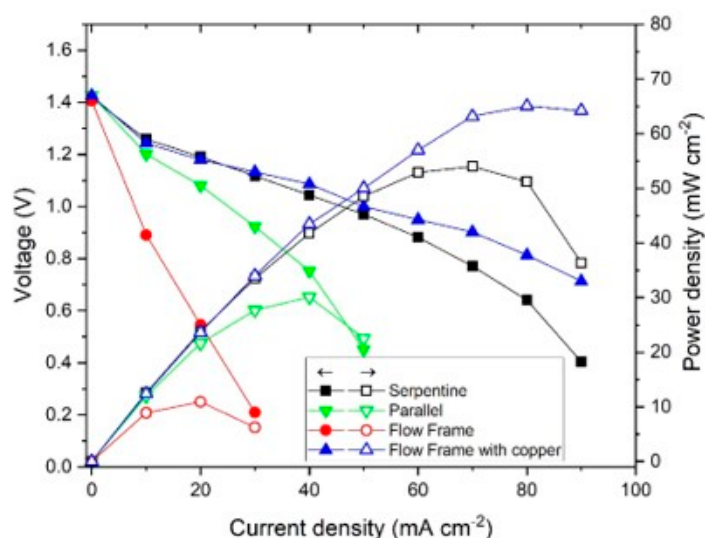

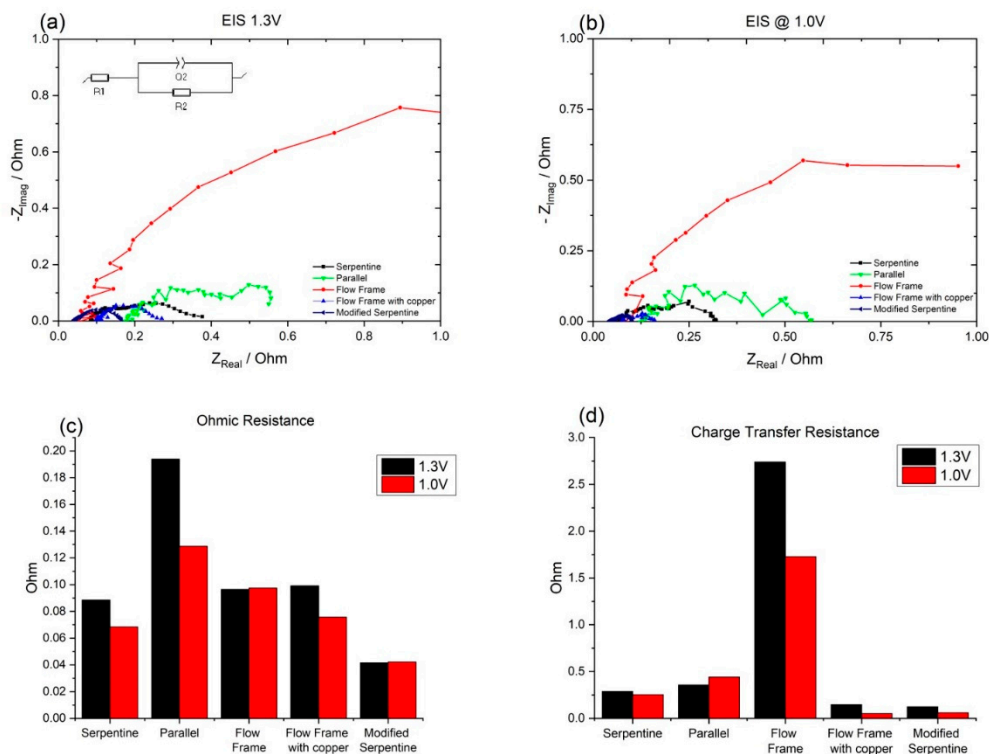**Figure 3.** Polarization (solid symbols) and power density (open symbols) curves of the different flow fields.

Figure 4. Nyquist plots for the different flow fields at (**a**) 1.3 V and (**b**) 1.0 V, and (**c**) graphs of ohmic and (**d**) charge transfer resistance.

Table 2. Active area and corrected geometric active area of each flow field.

Flow Field	Geometric Area (cm^2)	Area of Walls (cm^2)	Corrected Geometric Area (cm^2)
Serpentine	25	10.5	35.5
Parallel	25	14.4	39.4
Flow frame	25	0	25
Flow frame with copper base	25	0	25
Modified serpentine	25	17.82	42.9

Furthermore, as the zinc particles in the slurry are the active material, the presence of dead volume in the flow fields needs to be minimized to enhance the electrochemical performance. Hence, the slurry flow distribution in the serpentine and parallel flow fields was examined visually using a transparent end plate, as shown in Figure 5. The zinc slurries were circulated in both flow fields and observed for one minute. With the parallel flow field, dead volumes could be observed every 5–7 s, as shown in Figure 5b. Dead volumes can happen when the flow distribution is not optimal and stagnant slurry or air is present in the cell, which leads to a poorer electrochemical performance. On the other hand, no dead volumes were observed in the serpentine flow field. As serpentine flow fields force the zinc slurry to flow in a single direction, a continuous flow with low dead volumes can be achieved. On the other hand, parallel flow fields do not force the slurry in a single direction; thus, dead volumes are more likely to appear. This negatively affects the cell performance as zinc particles must react continuously to maintain a high electrochemical performance. The presence of dead volumes is probably why the parallel flow field presented a higher ohmic resistance than the serpentine one, which resulted in lower power densities.
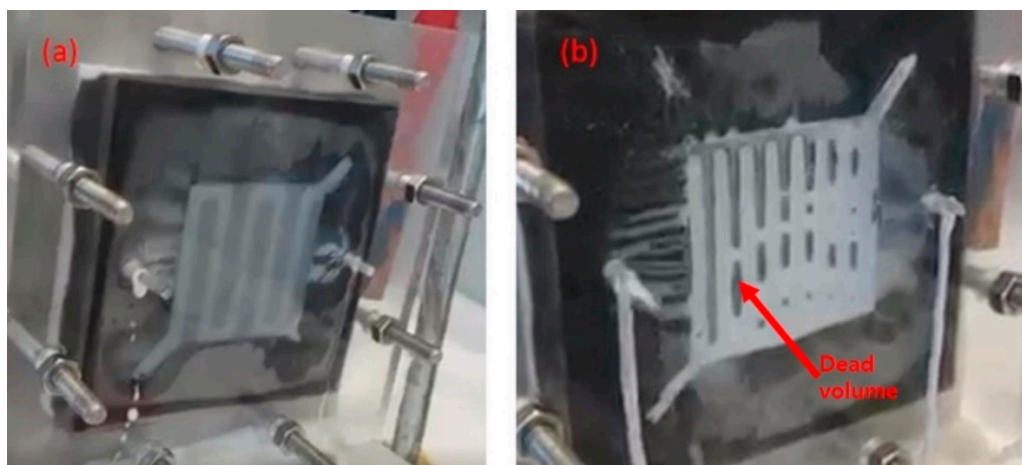
Figure 5. Distribution of the zinc slurry in the serpentine (**a**) and parallel (**b**) flow fields.

3.2. Effect of the Bipolar Plate Material

The material of the bipolar plate also plays an important role as shown by both polarization and EIS experiments. As copper is approximately 100 times more electrically conductive than graphite, it has the potential to improve the kinetics of zinc oxidation. Therefore, the PTFE flow frame was tested with a graphite bipolar plate and with a copper foil on top of the graphite plate. As the polarization curve in Figure 1 shows, by placing a copper foil on the top of the graphite plate, the current density at 0.7 V increased from 20 to 95 mA·cm^{-2}. Similarly, the maximum power density also increased from 10 to 60 mW·cm^{-2}, which was even greater than the graphite-based serpentine flow (55 mW·cm^{-2}). This suggests that the electrochemical performance is influenced by the material on the bipolar plate in contact with the zinc particles. Furthermore, the flow frames with copper-based and graphite-based bipolar plate showed similar ohmic resistances at 1.3 V, 0.09 Ω in both cases, and at 1.0 V, 0.07 Ω for copper-based and 0.09 Ω for the graphite-based plates, as shown in Figure 4c. Hence, by changing from a graphite to a copper plate, the ohmic resistance was reduced at higher current densities. Interestingly, as shown in Figure 4d, by using a copper-based flow frame, the charge transfer resistance was reduced from 2.7 to 0.15 Ω at 1.3 V and from 1.7 to 0.05 Ω at 1.0 V. Thus, it can be concluded that the zinc oxidation reaction is influenced by the choice of bipolar plate material.

The better performance can be related to the plating of zinc on the bipolar plate; it is widely reported in the literature that zinc can plate onto metals through an electroless process [35]. As the zinc particles get in contact with the copper plate, part of the zinc dissolves into zincate, while, at the same time, an equivalent part of zincate plates onto the copper as zinc. The copper is not consumed during this process, which results in a catalytic effect, where the presence of a copper plate enhances the zinc oxidation [36]. This leads to a situation were not only the zinc particles in contact with the bipolar plate will be discharged, but also the material that is continuously plated on top of it. Overall, this allows a higher electrochemical active area and subsequently causes a decrease in the charge transfer resistance.

3.3. Modifying a Flow Field with a New Material

The serpentine flow field showed the best performance among the graphite-based designs; moreover, the copper-based flow frame showed an enhanced electrochemical performance compared to the graphite-based one. Thus, a new design combining the advantages of the former was introduced to further improve the battery performance. A copper–nickel (70:30) alloy plate was selected as bipolar plate material to decrease the ohmic drop in the system. As the bipolar plate needs to maintain its properties during battery operation while a highly alkaline slurry is flowing, an alloy with high mechanical and corrosion resistance was chosen. Furthermore, as the corrected geometric active area proved to be an important factor for slurry-based flow batteries, a modified serpentine flow field with

higher corrected geometric area and better flow distribution was designed (Figure 1f). As a result, the new modified serpentine flow field with a copper–nickel-based bipolar plate showed a significant improvement in the zinc slurry air flow battery performance. As shown in Figure 6, the current density at 1.0 V was 140 mA·cm^{-2}, which was higher than the one measured for the other flow fields. The maximum power density for this flow field was 194 mW·cm^{-2}. Furthermore, the EIS results also indicated that the modified serpentine flow field had much lower ohmic and charge transfer resistances than the previous designs. As shown in Figure 4c, in both EIS conditions, the ohmic resistance was 0.04 Ω which is lower than that for any other flow fields. In addition, the charge transfer resistances, as shown in Figure 4d, were 0.12 Ω at 1.3 V and 0.05 Ω at 1.0 V, which were similar to or lower than the copper-based flow frame. This shows that, by modifying the flow fields by designing larger geometric active area and utilizing a copper–nickel alloy plate, both ohmic resistance and charge transfer resistance can be minimized. However, the metal bipolar plate could affect the durability of the battery; hence, a stability test of each material, as well as a constant current discharge curve, should be tested in future work.
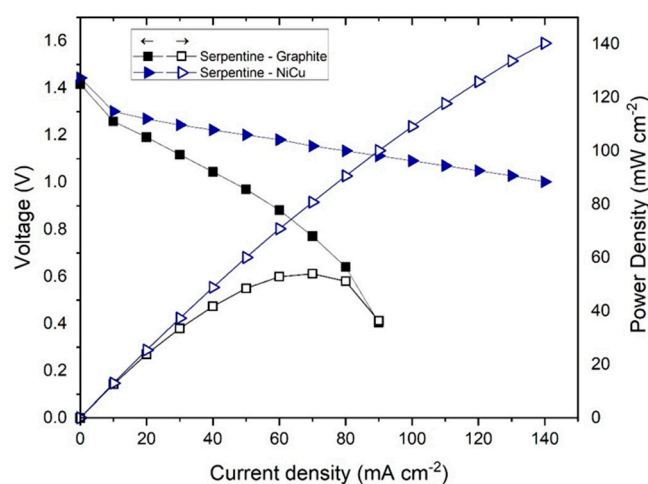

Figure 6. Comparison of the polarization (solid symbols) and power (open symbols) curves of the two serpentine flow fields with different materials.

4. Conclusions

In conclusion, different types of flow fields with different materials were introduced in this work to enhance the performance of zinc slurry air flow batteries. With graphite-based bipolar plates, the serpentine flow field showed higher power densities than the parallel flow field and the flow frame design. This is because the serpentine flow field has less dead volume than the parallel one, as well as a higher corrected geometric active area compared to the flow frame. Furthermore, when more conductive materials were used for the bipolar plate, such as copper or copper–nickel alloys, the electrochemical performance was greatly improved, reaching a power density of 194 mW·cm^{-2}. Consequently, for slurry-based flow batteries, a proper design of the flow field with high geometric active area and bipolar plate conductivity is important to achieve an enhanced battery performance.

Author Contributions: Conceptualization, N.H.C., D.d.O. and P.F.; Methodology, N.H.C.; Software, D.d.O.; Writing—original draft preparation, N.H.C.; Writing—review and editing, N.H.C, D.d.O. and P.F.; Supervision, P.F., K.P. and J.T. All authors have read and agreed to the published version of the manuscript.

References

1.　Caramia, V.; Bozzini, B. Materials science aspects of zinc-air batteries: A review. *Mater. Renew. Sustain. Energy* **2014**, *3*, 28. [CrossRef]

2.　Park, M.; Ryu, J.; Want, W.; Cho, J. Material design and engineering of next-generation flow-battery technologies. *Nat. Rev. Mater.* **2016**, *2*, 16080. [CrossRef]

3.　Han, X.; Li, X.; White, J.; Zhong, C.; Deng, Y.; Hu, W.; Ma, T. Metal-Air Batteries: From static to flow system. *Adv. Energy Mater.* **2018**, *8*, 1801396. [CrossRef]

4.　Bockelmann, M.; Kunz, U.; Turek, T. Electrically rechargeable zinc-oxygen flow battery with high power density. *Electrochem. Commun.* **2016**, *69*, 24–27. [CrossRef]

5.　Pan, F.; Wang, Q. Redox Species of Redox Flow Batteries: A Review. *Molecules* **2015**, *20*, 20499–20517. [CrossRef] [PubMed]

6.　Mainar, A.R.; Leonet, O.; Bengoechea, M.; Boyano, I.; de Meatza, I.; Kvasha, A.; Guerfi, A.; Blázquez, J.A. Alkaline aqueous electrolytes for secondary zinc–air batteries: An overview. *Int. J. Energy Res.* **2016**, *40*, 1032. [CrossRef]

7.　Li, Y.; Gong, M.; Liang, Y.; Feng, J.; Kim, J.-E.; Wang, H.; Hong, G.; Zhang, B.; Dai, H. Advanced zinc-air batteries based on high-performance hybrid electrocatalysts. *Nat. Commun.* **2013**, *4*, 1–7. [CrossRef] [PubMed]

8.　Jiratchayamaethasakul, C.; Srijaroenpramong, N.; Bunyangyuen, T.; Arpavate, W.; Wongyao, N.; Therdthianwong, A.; Therdthianwong, S. Effects of anode orientation and flow channel design on performance of refuelable zinc-air fuel cells. *J. Appl. Electrochem.* **2014**, *44*, 1205–1218. [CrossRef]

9.　McLarnon, F.R.; Cairns, E.J. The Secondary Alkaline Zinc Electrode. *J. Electrochem. Soc.* **1991**, *138*, 645. [CrossRef]

10.　Chakkaravarthy, C.; Waheed, A.K.A.; Udupa, H.V.K. Zinc-Air alkaline batteries—A Review. *J. Power Sources* **1981**, *6*, 203–228. [CrossRef]

11.　Li, Y.; Dai, H. Recent advances in zinc-air batteries. *Chem. Soc. Rev.* **2014**, *43*, 5257–5275. [CrossRef] [PubMed]

12.　Fu, J.; Cano, Z.P.; Park, M.G.; Yu, A.; Fowler, M.; Chen, Z. Electrically Rechargeable Zinc-Air Batteries: Progress Challenges and Perspectives. *Adv. Mater.* **2016**, *29*, 1604685. [CrossRef] [PubMed]

13.　Harting, K.; Kunz, U.; Turek, T. Zinc-air batteries: Prospects and challenges for future improvement. *Z. Phys. Chem.* **2012**, *226*, 151. [CrossRef]

14.　Sapkota, P.; Kim, H. Zinc air fuel cell a potential candidate for alternative energy. *J. Ind. Eng. Chem.* **2009**, *15*, 445–450. [CrossRef]

15.　Mainar, A.; Iruin, E.; Colmenares, L.; Blázquez, J.; Grande, H.-J. Systematic cycle life assessment of a secondary zinc–air battery as a function of the alkaline electrolyte composition. *Energy Sci. Eng.* **2018**, *6*, 174–186. [CrossRef]

16.　Kupsch, C.; Feierabend, L.; Nauber, R.; Büttner, L.; Czarske, J. Ultrasound flow investigations at a zinc-air flow battery model. In Proceedings of the ICEFM 2018 Munich, Munich, Germany, 2–4 July 2018.

17.　Ma, H.; Wang, B.; Fan, Y.; Hong, W. Development and Characterization of an Electrically Rechargeable Zinc-Air Battery Stack. *Energies* **2014**, *7*, 6548–6557. [CrossRef]

18.　Ma, Z.; Pei, P.; Wang, K.; Wang, X.; Xu, H.; Liu, Y.; Peng, G. Degradation characteristics of air cathode in zinc air fuel cells. *J. Power Sources* **2015**, *274*, 56–64. [CrossRef]

19.　Yang, D.; Zhang, L.; Yan, X.; Yao, X. Recent Progress in Oxygen Electrocatalysts for Zinc–Air Batteries. *Small Methods* **2017**, *1*, 1700209. [CrossRef]

20.　Mainar, A.; Iruin, E.; Colmenares, L.; Kvasha, A.; Meatza, I.; Bengoechea, M.; Leonet, O.; Boyano, I.; Zhang, Z.; Blazquez, J. An overview of progress in electrolytes for secondary zinc-air batteries and other storage systems based on zinc. *J. Energy Storage* **2018**, *15*, 304–328. [CrossRef]

21.　Liu, S.; Han, W.; Cui, B.; Liu, X.; Sun, H.; Zhang, J.; Lefler, M.; Licht, S. Rechargeable Zinc Air Batteries and Highly Improved Performance through Potassium Hydroxide Addition to the Molten Carbonate Eutectic Electrolyte. *J. Electrochem. Soc.* **2018**, *165*, A149–A154. [CrossRef]

22.　Shi, Y.; Eze, C.; Xiong, B.; He, W.; Zhang, H.; Lim, T.M.; Ukil, A.; Zhao, J. Recent development of membrane for vanadium redox flow battery applications: A review. *Appl. Energy* **2019**, *238*, 202–224. [CrossRef]

23.　Tsehaye, M.T.; Alloin, F.; Iojoiu, C. Prospects for Anion-Exchange Membranes in Alkali Metal–Air Batteries. *Energies* **2019**, *12*, 4702. [CrossRef]

24. Weber, A.Z.; Mench, M.M.; Meyers, J.P.; Ross, P.N.; Gostick, J.T.; Liu, Q. Redox flow batteries: A review. *J. Appl. Electrochem.* **2011**, *41*, 1137–1164. [CrossRef]

25. Darling, R.M.; Perry, M.L. The Influence of Electrode and Channel Configuration on Flow Battery Performance. *J. Electrochem. Soc.* **2014**, *161*, A1381–A1387. [CrossRef]

26. Houser, J.; Clement, J.; Pezeshki, A.; Mench, M.M. Influence of architecture and material properties on vanadium redox flow battery performance. *J. Power Sources* **2016**, *302*, 369–377. [CrossRef]

27. Houser, J.; Pezeshki, A.; Clement, J.T.; Aaron, D.; Mench, M.M. Architecture for improved mass transport and system performance in redox flow batteries. *J. Power Sources* **2017**, *351*, 96–105. [CrossRef]

28. Ke, X.; Alexander, J.I.D.; Prahl, J.M.; Savinell, R.F. Flow distribution and maximum current density studies in redox flow batteries with a single passage of the serpentine flow channel. *J. Power Sources* **2014**, *270*, 646. [CrossRef]

29. Ke, X.; Alexander, J.I.D.; Prahl, J.M.; Savinell, R.F. Mathematical modeling of electrolyte flow in a segment of flow channel over porous electrode layered system in vanadium flow battery with flow field design. *J. Electrochim. Acta* **2017**, *223*, 124. [CrossRef]

30. Ke, X.; Prahl, J.M.; Alexander, J.I.D.; Wainright, J.S.; Zawodzinski, T.A.; Savinell, R.F. Rechargeable redox flow batteries: Flow fields, stacks and design considerations. *Chem. Soc. Rev.* **2018**, *47*, 8721–8743. [CrossRef]

31. Xu, Q.; Zhao, T.S.; Leung, P.K. Numerical investigations of flow field designs for vanadium redox flow batteries. *Appl. Energy* **2013**, *105*, 47–56. [CrossRef]

32. Xu, Q.; Zhao, T.S.; Zhang, C. Performance of a vanadium redox flow battery with and without flow field. *Electrochim. Acta* **2014**, *142*, 61–67. [CrossRef]

33. Dennison, C.R.; Agar, E.; Akuzum, B.; Kumbur, E.C. Enhancing Mass Transport in Redox Flow Batteries by Tailoring Flow Field and Electrode Design. *J. Electrochem. Soc.* **2016**, *161*, A5163–A5169. [CrossRef]

34. Cho, K.T.; Ridgway, P.; Haussener, W.S.; Battaglia, V.; Srinivasan, V. High performance hydrogen/bromine redox flow battery for grid-scale energy storage. *J. Electrochem. Soc.* **2012**, *159*, A1806–A1815. [CrossRef]

35. Brenner, A. *Electrodeposition of Alloys: Principles and Practice*; Academic Press: Cambridge, MA, USA, 1963; pp. 411–496.

36. Vijayaratnam, V.; Natter, H.; Grandthyll, S.; Neurohr, J.U.; Jacobs, K.; Müller, F.; Hempelmann, R. Unwanted electroless zinc plating on current collectors in zinc air batteries. *arXiv* **2017**, arXiv:1706.05929.